Journal of Volcanology and Geothermal Research 438 (2023) 107807

Contents lists available at ScienceDirect

Journal of Volcanology and Geothermal Research

journal homepage: www.journals.elsevier.com/journal-of-volcanology-and-geothermal-research

Quantification of CO_2 degassing and atmospheric dispersion at Caldeiras da Ribeira Grande (São Miguel Island, Azores)

Fátima Viveiros [a,b], Eleonora Baldoni [a,b], Silvia Massaro [c,d,*], Manuel Stocchi [c], Antonio Costa [d], Stefano Caliro [e], Giovanni Chiodini [d], César Andrade [a,f]

[a] IVAR - Research Institute for Volcanology and Risks Assessment, University of the Azores, Portugal
[b] FCT - Faculty of Sciences and Technology, University of the Azores, Ponta Delgada, Portugal
[c] Department of Earth and Geo-environmental Sciences, University of Bari, Italy
[d] INGV - National Institute of Geophysics and Volcanology, Bologna, Italy
[e] INGV - National Institute of Geophysics and Volcanology, Naples, Vesuvian Observatory, Italy
[f] CIVISA - Centre for Information and Seismovolcanic Surveillance of the Azores, University of the Azores, Portugal

ARTICLE INFO

Keywords:
Azores Archipelago
Soil CO_2 diffuse degassing
Atmospheric gas dispersion
Model validation
Hazard assessment

ABSTRACT

Caldeiras da Ribeira Grande is one of the degassing areas of Fogo, a trachytic central volcano located at São Miguel Island (Azores archipelago). Recently, new steam emissions, soil CO_2 and temperature anomalies developed towards the inhabited area, causing high indoor CO_2 values and affecting the vegetation and several small animals that were found dead in depressions and low-ventilated zones. During July–August 2021, a soil CO_2 flux survey was carried out on the north flank of the volcano, estimating a soil gas release of at least 40 t d^{-1} (excluding the contribution of the fumaroles) over an area of ~0.27 km^2. Two populations for the CO_2 released were found, highlighting the biogenic and volcanic-hydrothermal origins. General NW-SE diffuse degassing structures (DDS) were identified, in agreement with the tectonic lineaments previously recognized in the area. In this regard, we investigated the passive gas dispersion in the atmosphere at Caldeiras da Ribeira Grande performing a model validation aimed to estimate the fumarolic gas flux at source and the potential hazard for human and animal lives posed by CO_2. Numerical simulations were carried out with the DISGAS-2.3, a 3D Eulerian advection-diffusion model, and the relative outputs processed through the VIGIL-1.3 workflow able to provide probabilistic long-term CO_2 concentration maps, considering a meteorological variability over the last 30 years (1991–2020) taken from the ECMWF ERA5 reanalysis dataset. A best-fit between observed and simulated CO_2 concentrations allowed us to estimate the total gas flux of the area (~209 t d^{-1}) obtained by scaling the soil CO_2 gas flux by a factor 30. Such an estimate is composed of ~174 t d^{-1} as unknown fumarolic and ~ 35 td^{-1} as diffuse contribution, in a good agreement with measurements.

Although the present-day CO_2 concentration at 0.3 m height cannot be considered to raise serious concerns for human health, we reasonably infer that the death of small animals may be due to local conditions of CO_2 accumulation or to the presence of H_2S. The current study highlights the relevance of coupling gas flux maps, concentration data, and gas dispersion modeling to obtain robust estimation of gas fluxes, including the fumarolic contribution, and identify zones potentially impacted by dangerous concentrations of volcanic gases, which are relevant for land-use planning and hazard assessment in case of renewed escalations of volcanic activity.

1. Introduction

Volcanoes can release high amount of volatiles to the atmosphere, even during quiescent periods and through diffuse degassing, as showed by several studies in the last three decades (e.g., Allard et al., 1991; Chiodini et al., 1996, 1998; Bergfeld et al., 2001; Brombach et al., 2001; Cardellini et al., 2003; Notsu et al., 2005; Viveiros et al., 2010; Werner et al., 2019; Biagi et al., 2022; Fischer and Aiuppa, 2020; Andrade et al., 2021). Gases (mainly CO_2, ^{222}Rn, and H_2S) released in the diffuse degassing areas can also pose a threat for the population, being soil degassing one of the permanent hazards in inhabited areas (e.g., Beaubien et al., 2003; Barberi et al., 2007, 2019; Viveiros et al., 2015a,

* Corresponding author at: Department of Earth and Geo-environmental Sciences, University of Bari, Italy
E-mail address: silvia.massaro@uniba.it (S. Massaro).

https://doi.org/10.1016/j.jvolgeores.2023.107807
Received 1 December 2022; Received in revised form 5 April 2023; Accepted 14 April 2023
Available online 19 April 2023

2016).

For the particular case of CO_2 which is odorless and colorless, it can start affecting human health at concentrations above 5000 ppm (NIOSH, 2007). The short time exposure limit (STEL) for a CO_2 concentration of 30,000 ppm has been fixed at 15 min and above that concentration exposure symptoms increase the breathing normal rate, narcotic effects and headaches. Above 150,000 ppm, CO_2 concentration in the air may cause death acting as asphyxiant (Le Guern et al., 1982; Blong, 1984; Wong, 1996; Williams-Jones and Rymer, 2000; NIOSH, 2007; Costa and Chiodini, 2015; Viveiros et al., 2015b). In addition, as CO_2 is denser than the air at STP conditions, it can accumulate in depressed zones and/or confined spaces, contributing to hazardous gas concentrations (e.g., Costa and Chiodini, 2015; Folch et al., 2009, 2017; Permentier et al., 2017).

Several studies (Barberi et al., 2007, 2019; Viveiros et al., 2009, 2010, 2015b, 2016; Carapezza et al., 2022) have shown that buildings located in CO_2 diffuse degassing zones may accumulate indoor hazardous concentrations of gas, reaching in some cases lethal levels. In fact, lethal CO_2 concentrations were observed for several periods in the indoor CO_2 time series recorded at some dwellings in the Azores archipelago, confirming that in diffuse degassing areas the population may be at permanent risk of exposure to CO_2 (Viveiros et al., 2009, 2015b, 2016). In the Azores archipelago the most tragic accident caused by CO_2 in periods of quiescence occurred in 1992, with the deaths of two tourists inside the Furna do Enxofre lava cave in Graciosa Island, where air CO_2 concentrations higher than 15 vol% were measured (Gaspar et al., 1998; Viveiros et al., 2015b).

Several studies have also been developed in the last decade to evaluate outdoor CO_2 dispersion (e.g., Costa et al., 2005; Folch et al., 2009, 2017; Granieri et al., 2013; Pedone et al., 2017; Massaro et al., 2021; Dioguardi et al., 2022).

For gas passively driven by wind advection and atmospheric turbulence, models based on generalized advection-diffusion equations can be used. Among these, we consider DISGAS (Costa et al., 2005; Costa and Macedonio, 2016), a Eulerian model coupled with a mass-consistent wind model (Douglas et al., 1990). It needs as input data topography, average wind on the computational domain, atmospheric stability information and sources emission rates. The outputs consist of gas concentration grids at the users-selected timesteps and levels from the ground.

Granieri et al. (2013) applied DISGAS to the La Solfatara di Pozzuoli volcano (Italy) in order to simulate the passive CO_2 dispersion and evaluate the potential hazards in the surrounding city of Naples. More recently, Massaro et al. (2022) verified the forecasting capability of DISGAS through the observed CO_2 concentrations acquired during June 2020.

In this work, we model the outdoor gas dispersion at Caldeiras da Ribeira Grande in the Azores archipelago, where present-day volcanic activity is marked by several low-temperature fumarolic fields, steaming ground, thermal and cold CO_2-rich springs and soil diffuse degassing areas (Caliro et al., 2015; Viveiros et al., 2010, 2015a).

A new degassing area developed in the north flank of Fogo Volcano (São Miguel Island) during 2010 due to the drilling of a geothermal well. In this case, new fumarolic areas appeared in the surroundings of a pre-existing fumarolic field, the Caldeiras da Ribeira Grande fumaroles. Together with steam emissions, soil CO_2 and temperature anomalies developed in the area (Viveiros et al., 2021; Pereira et al., 2022). The degassing phenomena also extended towards an inhabited area, the Caldeiras da Ribeira Grande site, and caused not only high indoor CO_2 values, but also affected the vegetation and several small animals that were found dead in depressions and low-ventilated zones.

As known, fumarolic fluxes can have highly variable emissions, both in terms of the composition and the rate of the gases being emitted (e.g., Werner et al., 2000; Pedone et al., 2015). This variability poses difficulties to obtain accurate and representative measurements of the fumarolic flux, considering the technical limitations of the instruments (such as gas analyzers and thermal cameras), whose accuracy can be affected by the wind, humidity, and equipment drift.

Based on this, the current study, for the first time, aims to indirectly estimate the fumarolic flux of CO_2 in the Caldeiras da Ribeira Grande area by comparing the results of numerical gas dispersal simulations with the available sporadic measurements of atmospheric CO_2 concentrations. Then, an evaluation of the related potential hazards for human and animal health is also provided.

The simulations are carried out with DISGAS-2.3 (Costa and Macedonio, 2016) model and the outputs processed through a Python automatic workflow, VIGIL-1.3 (Dioguardi et al., 2022), in order to provide probabilistic long-term CO_2 and H_2S concentration maps based on the soil CO_2 flux survey of July/August 2021. The current study can be also used to define potential gas hazardous zones, in case of gas flux increase in the area.

2. Characterization of the study area

The Azores archipelago is in a shallow bathymetry zone within the Atlantic Ocean, in the triple junction of the Eurasia, Nubia and North America plates (Carmo et al., 2015 and references therein; Fig. 1a). São Miguel is the biggest island and is in the western group of islands of the Azores Archipelago. The island has an east-west elongated shape and is formed by three quiescent polygenetic central volcanoes with summit calderas (Sete Cidades, Fogo, Furnas; Fig. 1b), linked by two active fissure zones (Gaspar et al., 2015). São Miguel is shaped by several tectonic structures with a dominant NW-SE trend, including the Ribeira Grande *graben*, and WNW-ESE, with two groups of faults dipping 60°-90° to NE and SW (Carmo et al., 2015).

Fogo Volcano is in the central part of the island and started to form nearly 200 ka BP (Wallenstein et al., 2015). The volcano is dominated by an intra caldera lake, which according to studies carried out by Andrade et al. (2020), showed absence of deep-derived CO_2. There were five trachytic explosive eruptions during the last 5 ka, and two of them occurred in historical times (Wallenstein et al., 2015).

Hydrothermal manifestations are mainly found on the north flank of the volcano and are associated with the NW-SE Ribeira Grande graben. The main hydrothermal manifestations comprise Caldeiras da Ribeira Grande (the studied area; Fig. 1c), Caldeira Velha and Pico Vermelho, which show low temperature fumaroles and steaming ground (Caliro et al., 2015). Recent studies suggest that the reservoir feeding Caldeiras da Ribeira Grande fumaroles has temperatures around 256 °C (Pereira et al., 2022). Thermal, cold CO_2-rich springs and diffuse degassing areas are also found in the north flank of Fogo Volcano (Cruz and França, 2006; Viveiros et al., 2015b). Due to the diffuse CO_2, some dwellings located on the north flank of the volcano (Ribeira Seca village and Caldeiras da Ribeira Grande site) were previously affected by high indoor CO_2 concentrations (Viveiros et al., 2015b). In the Caldeiras da Ribeira Grande, a permanent monitoring system was installed in 2012 to evaluate indoor air CO_2 concentration for health risks assessment purposes (Viveiros et al., 2021).

From a meteorological point of view, the Azores climate is oceanic temperate, being marked by several local microclimates, which depend on factors such as altitude, distance from the sea, shape of the islands, and soil occupation (Bettencourt, 1979). Inter-annual and inter-seasonal variability of the rainfall patterns in the archipelago are shown by the significant differences between the "rainy season" that extends from October to March (with about 70% of the annual precipitation) and the "dry season" with the minimum rainfall in July (Bettencourt, 1979; Marques et al., 2007).

3. Methodology

3.1. Sampling

The degassing survey was performed at Caldeiras da Ribeira Grande

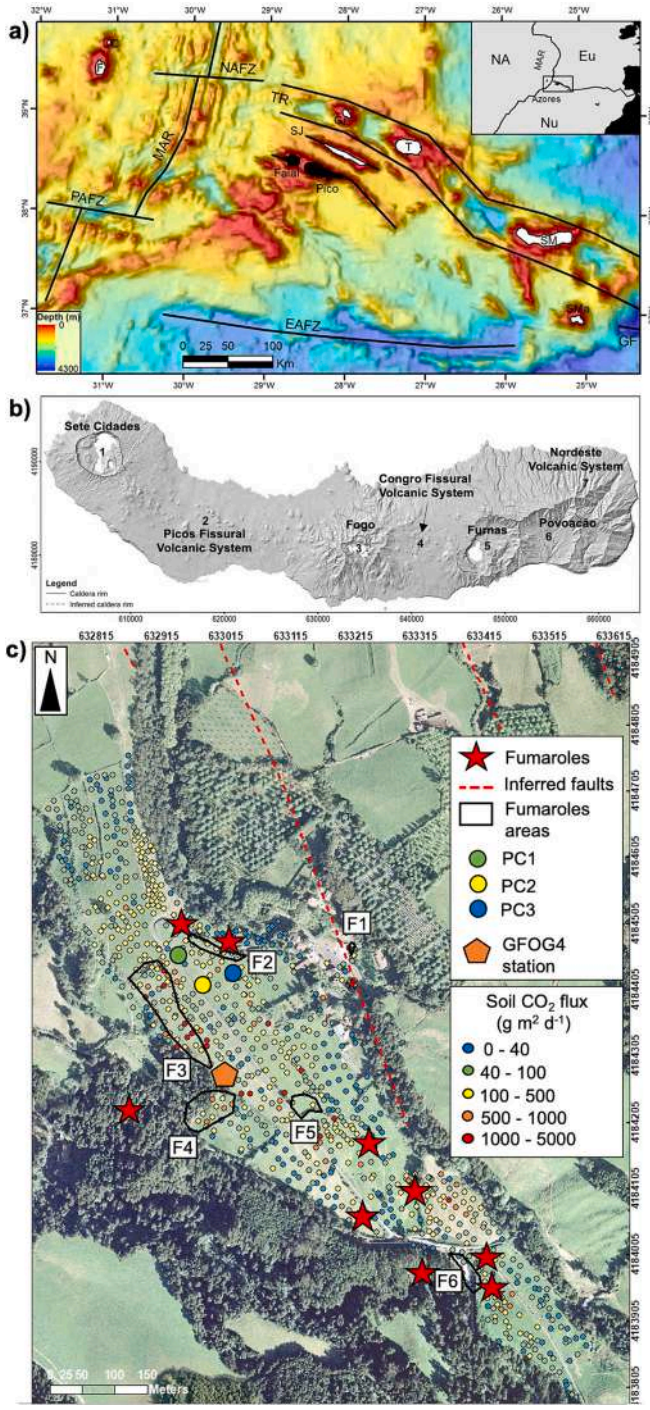

Fig. 1. a) Regional setting of the Azores archipelago within the North American (NA), Eurasian (Eu), and Nubian (Nu) triple junction. The top right inset depicts the location of the Azores archipelago in the North Atlantic Ocean. Tectonic structures: MAR, Mid-Atlantic Ridge; NAFZ, North Azores Fracture Zone; PAFZ, Princess Alice Fracture Zone; EAFZ, East Azores Fracture Zone; GF, Gloria Fault; Terceira Rift (TR). Islands: C, Corvo; F, Flores; SJ, São Jorge; Gr, Graciosa; T, Terceira; SM, São Miguel; SMa, Santa Maria. Faial and Pico Islands are highlighted in black. Solid lines correspond to major structures/faults (modified after Quartau et al., 2015); b) São Miguel island with its six volcanic centres (modified after Carmo et al., 2015); c) CO_2 flux measurement locations and main fumarolic emissions located in Caldeiras da Ribeira Grande, signed as F1,2,3,4,5,6. Datum = World Geodetic System (WGS) 84. PC1,2,3 correspond to the three control points.

in 2021. A total of 830 sites were sampled (Table A2, Appendix A) in an area with approximately 0.27 km^2, following a grid of about 20 m (Fig. 1c). The measured variables were soil CO_2 fluxes, CO_2 concentrations (0.30 m and 1.50 m height) and temperature (soil and air).

Data were collected in 11 days during July–August 2021, in dry weather conditions, to avoid the potential influence of meteorological conditions on the soil CO_2 fluxes (e.g., Viveiros et al., 2008, 2010). In addition, data recorded at the permanent soil CO_2 flux station GFOG4 were used to check intra-survey variability, and three control sites were selected and measured (for CO_2 flux and concentrations) every day during the surveyed period (Appendix A, Fig. A2). GFOG4 has also coupled a meteorological station with several sensors such as barometric pressure, air temperature, air relative humidity, wind speed and direction, rainfall, soil water content and soil temperature. Thermo-hygrometers and wind sensors are set about 1 m above the ground, whereas soil water content and soil temperature sensors give measurements at a depth of about 0.30 m (Oliveira et al., 2018).

At each site, the soil temperatures were measured at depths in between 5 and 10 cm depending on the soil hardness, while the air temperatures were taken at soil level and 0.30 m above the soil. Temperature was measured on the same points of the CO_2, always after the gas flux measurements, using a portable thermocouple (thermometer Testo 925 with resolution of 0.1 °C for the 50–200 °C range).

CO_2 fluxes and concentrations were measured using two portable instruments (manufactured by West Systems, Italy). The instruments perform flux measurements based on the accumulation chamber method (Chiodini et al., 1998). The two instruments (WS1214 and WS1018) were equipped with LICOR LI-820 CO_2 detectors, with 20,000 ppm as full scale. Previous studies (Chiodini et al., 1998) reported a reproducibility around 10% for the CO_2 fluxes ranging between 10 and 10,000 g m^{-2} d^{-1}. According to Carapezza and Granieri (2004) the uncertainty increases to 24% in low soil CO_2 flux areas. To have no discrepancy between the measurements taken by the two instruments, the calibrations of the fluxmeters have been previously done in the laboratory. In addition, soil CO_2 fluxes were measured in the same sites using both instruments and varied <20%.

CO_2 flux measurements were not done in the steam emissions sites to avoid any damage of the instruments due to condensation in the sampling line.

3.2. CO_2 flux statistical analyses

The Sinclair procedure (Sinclair, 1974) was applied to the soil CO_2 fluxes to define potential flux populations that can represent different CO_2 sources (Fig. 2). The CO_2 flux and concentration maps, as well as the soil temperature were elaborated using the sequential Gaussian simulations (sGs) (Deutsch and Journel, 1998; Cardellini et al., 2003).

The sGs method, which uses the sGs algorithm (Deutsch and Journel, 1998), consists of the production of numerous simulations of the spatial distribution of the attribute (CO_2 flux, air CO_2 concentrations at 0.3 m and 1.50 m height, and soil temperature, in this study). Stochastic simulation produces realizations that respect the original data statistics (e.g., histograms, variograms) without smoothing the extreme values (Cardellini et al., 2003).

Since the collected data do not follow the normal multi-Gaussian distribution, data were transformed into normal distribution by a normal score transform (Deutsch and Journel, 1998; Cardellini et al., 2003). A simulated value at one location is randomly selected from the normal distribution function defined by the kriging mean and variance based on the neighborhood values. The simulation is sequential and conditional, meaning that the simulated value at each point is conditioned both on the original data and on the previously simulated values (Deutsch and Journel, 1998; Goovaerts, 1999). The process is repeated until all points are simulated. Interpolation criteria were based on the experimental variograms, computed and modeled for each data set (see Fig. 3). The resulting E-type flux map, which shows the “expected” value

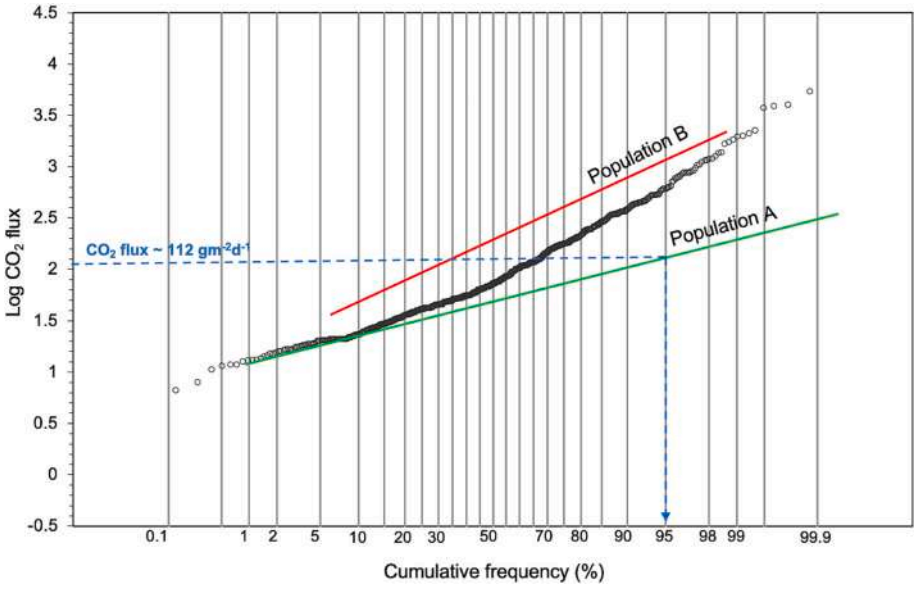

Fig. 2. Probability plot of soil CO_2 flux at Caldeiras da Ribeira Grande (data referenced in Table 3). The dashed blue line corresponds to the 95th percentile of population "A". (For interpretation of the references to colour in this figure legend, the reader is referred to the web version of this article.)

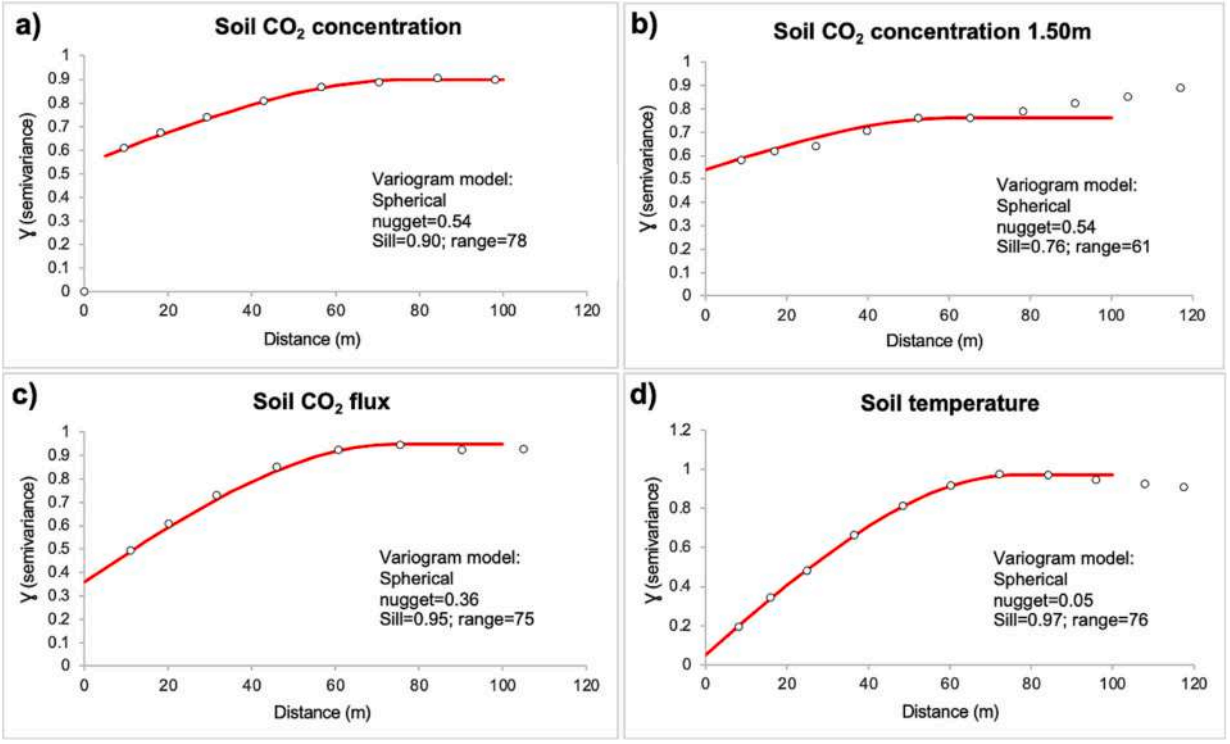

Fig. 3. Experimental (white dots) and modeled (red line) variograms for the different data sets. (For interpretation of the references to colour in this figure legend, the reader is referred to the web version of this article.)

at any location obtained through a point-wise linear average of all 100 simulations (Deutsch and Journel, 1998; see Fig. 4a) was then used as input data to produce CO_2 dispersion simulations.

3.3. Physical model and numerical simulations

The physics of atmospheric gas dispersion can be dominated by advection-diffusion (i.e., by the atmospheric wind field, turbulence and gas concentration gradient) or gravity-driven (i.e., governed by buoyancy forces). The choice between these two regimes can be done by calculating the Richardson number *Ri* relative to the system:

$$Ri = \frac{1}{V^2}\frac{(g'q)^{2/3}}{R^{2/3}} \quad (1)$$

where $g' = g(\rho_g - \rho_a)/\rho_a$ is the reduced gravity acceleration (being g the gravity acceleration, ρ_a and ρ_g the air and the gas density respectively), q is the volumetric flow rate, R the plume size, and V is the wind intensity at the reference altitude (i.e., 3 or 10 m). For $Ri < 0.25$ the flow is substantially advection-diffusion driven whereas for $Ri > 1$ is mainly

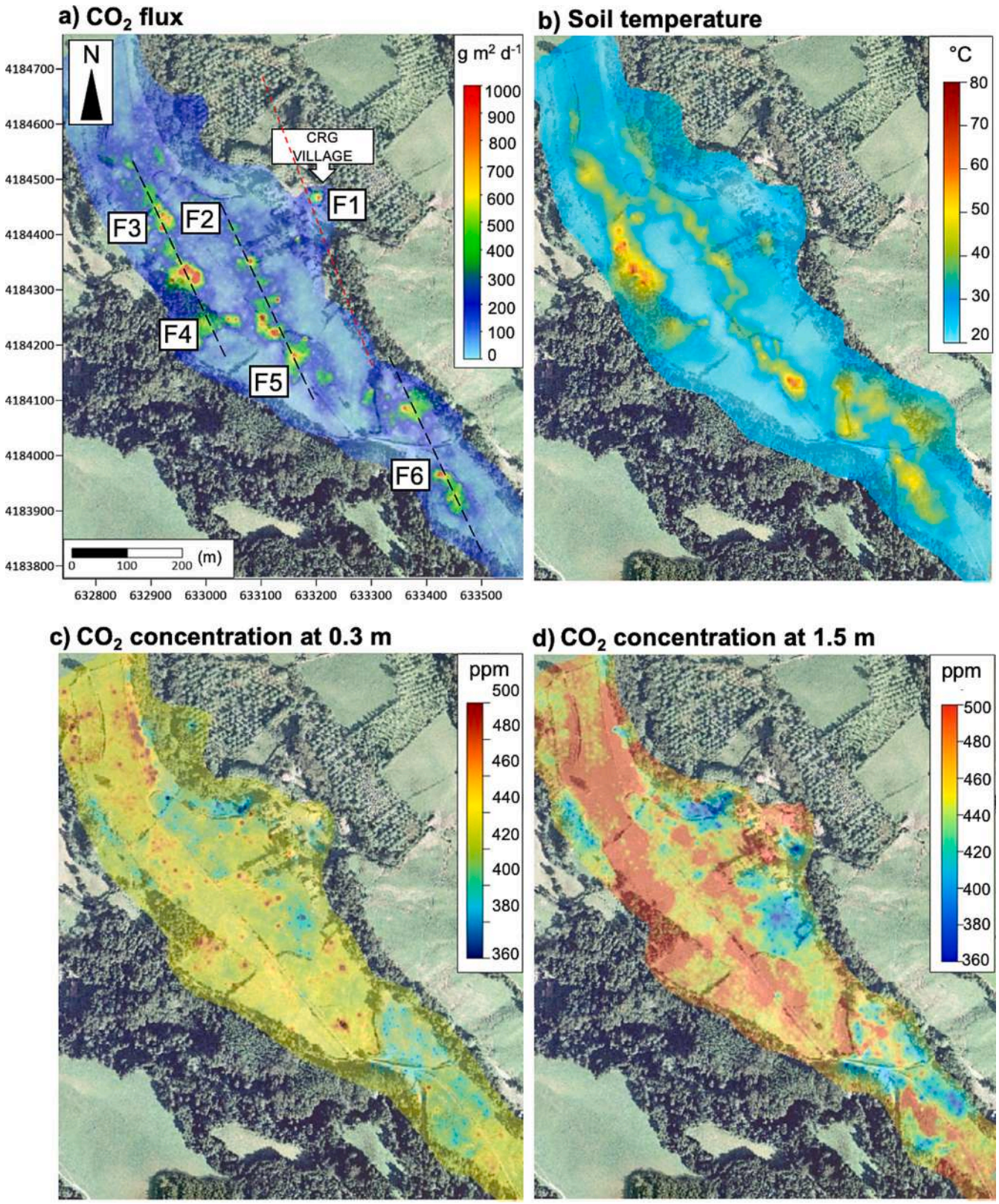

Fig. 4. a) The E-type of soil CO_2 flux map (g $m^{-2}d^{-1}$), b) soil temperature (°C), c) CO_2 concentration at 1.50 m height (ppm) and d) CO_2 concentration at 0.30 m height (ppm) for Caldeiras da Ribeira Grande. Black dashed lines on CO_2 flux map represent lineaments associated to the gas anomalies (a), while a tectonic feature inferred by Carmo et al. (2015) is shown as red. Caldeiras da Ribeira Grande village is indicated as CRG Village. F1,2,3,4,5,6 represent the main fumarolic fields corresponding to the DDS as related to Fig. 1c. (For interpretation of the references to colour in this figure legend, the reader is referred to the web version of this article.)

density driven (Cortis and Oldenburg, 2009; Costa et al., 2013; Costa and Macedonio, 2016). In our case, we considered the averaged values of gas emissions temperature and atmospheric pressure at Caldeiras da Ribeira Grande. As volumetric flow we considered the diffuse flux acquired during the gas survey (~40 t d^{-1}) while the plume radius was ideally set considering the averaged major axis of the ideal ellipse that includes the gas measurements. The reference parameters are reported in Table 1. In this way, the estimated *Ri* value is ~0.04–0.09, therefore the CO_2 flow has a passive regime. For this reason, DISGAS was the numerical model used in this study.

The simulations were run through VIGIL-1.3 (Dioguardi et al., 2022), an automatized probabilistic workflow which uses two Eulerian codes for passive and/or density driven gas dispersion (DISGAS-2.3; Costa and Macedonio, 2016; TWODEE-2- 2.6; Hankin and Britter, 1999; Folch et al., 2009) over large and complex topographic domains; these models are coupled with the mass-consistent Diagnostic Wind Model (DIAGNO; Douglas et al., 1990) that creates a 3D null-divergence wind field over a complex topography, starting from user-defined initial values. VIGIL manages the following steps: 1) retrieval of the meteorological data; 2) execution of the numerical simulation; 3) post-processing of the results. It can run gas dispersal simulations in both reanalysis and forecast mode. In the former mode, the user can download and process local weather station data or reanalysis data relative to the domain of interest from the ECMWF ERA5 database (Hersbach et al., 2018). The ERA5 reanalysis weather data have a temporal resolution of 1 h, 30 km horizontal resolution and 37 vertical levels from the ground up to 1 mbar pressure level. From the ECMWF ERA5 dataset, it is also possible to retrieve forecast data from the Integrated Forecasting System (IFS).

VIGIL has been recently applied to the case of the quasi-permanent degassing of La Soufrière volcano (Guadeloupe, Lesser Antilles; Massaro et al., 2021), providing prototypical tests aimed to validate the modeling of gas dispersal from a hazard perspective (in other words, its ability in reproducing the correct order of magnitude and variability of gas concentrations dispersed from the summit dome fumaroles).

In this study, the numerical simulations were run to perform a model validation aimed at evaluating whether the estimated fluxescould reproduce the measured CO_2 concentrations (see Section 4.3). We also investigated how the diffuse and fumarolic sources could impact the interested area providing long-term statistical CO_2 and H_2S concentration maps (see Section 4.4), obtained by performing 1000 gas dispersal simulations through VIGIL. In case future increases of gas fluxes push the transport towards a gravity driven regime, similar analysis could be performed using a suitable gas transport model (e.g., Hankin and Britter, 1999; Folch et al., 2017).

The model validation was carried out comparing the observed and simulated CO_2 concentration at 43 tracking points in the investigated area (Fig. 5a). The computational domain is represented by a 2D regular grid of 874 × 672 points (spacing ~16.5 m in both directions; Fig. 5a), while the topography is represented by a 10 m resolution DEM (courtesy SIG team, IVAR).

For gas sources, applied a resampling of the diffuse fluxes using ©Surfer software using a resolution of 50 m (see section 3.1). Since the accumulation chamber method reaches saturation levels at fumarolic sites and the infrared detector can be damaged by the steam (hence the method is not applicable), we indirectly inferred the fumarolic flux by scaling the diffusive flux measured in proximity to the fumarolic area (red stars in Fig. 1c).

We considered different scaling factors, multiplying the diffuse flux by 10 up to 1000 to find the best correlation with observed CO_2 concentration data, avoiding an underestimation of the fumarolic contribution in the modeling.

Table 1
Parameters used to calculate the Richardson number.

Symbol	Description	Value
ρ_g	gas density at T = 80.7 °C and P = 993 mbar (kg m^{-3})	1.48
ρ_a	air density at T = 80.7 °C and P = 993 mbar (kg m^{-3})	0.9
q	volumetric flow (m^3 s^{-1})	0.32
R	plume radius (m)	75–500
V	wind velocity at reference altitude (m/s)	1

4. Results

4.1. Descriptive statistics

At Caldeiras da Ribeira Grande soil CO_2 fluxes ranged from 6.6 g m^{-2} d^{-1} to 5427 g m^{-2} d^{-1}, and the highest values are mainly related to anomalous soil temperature (maximum measured value was 80.7 °C; Table 2). PC3 (control point 3; Fig. 1c) has shown the highest soil CO_2 flux values (average ~ 145 g m^{-2} d^{-1}), considering the three sites selected and the coefficient of variation (CV) of 0.25. PC1 (Fig. 1c) has shown the highest soil CO_2 flux variability (CV = 0.49), and corresponds to the lowest CO_2 fluxes from the control sites. Environmental variables showed low variability during the surveyed period when compared to the soil CO_2 fluxes (Table A2, Appendix A). Air CO_2 concentrations reached maximum values at 0.3 m (1956 ppm), slightly higher than maximum concentrations measured at 1.5 m (960 ppm).

4.2. Mapping and quantification of soil CO_2 degassing

Soil CO_2 flux values from Caldeiras da Ribeira Grande were modeled using the procedure proposed by Sinclair (1974), as a combination of two overlapping lognormal populations (Fig. 2). This bimodal distribution with an inflection point at the 59th cumulative percentile suggests the existence of multiple sources (biogenic and volcanic-hydrothermal) that overall feed soil CO_2 diffuse degassing.

The estimated mean and the proportion of partitioned populations are reported in Table 3. Population referred to as "A" is characterized by lower CO_2 fluxes (mean ~ 58.6 g m^{-2} d^{-1}), when compared to population "B", with a mean of ~377.4 g m^{-2} d^{-1}. If population "A"is assumed to be connected to biological activity in the soil, the choice of the 95th percentile of this population as cut-off for the biogenic (background) contribution (as previously applied by Viveiros et al., 2010, 2020; Andrade et al., 2016) results on a threshold of ~112 g m^{-2} d^{-1} (Fig. 2). This threshold is quite high compared with the values suggested to other degassing sites of the Azores archipelago, where threshold CO_2 fluxes associated with biogenic production ranged between 25 and 45 g $m^{-2}d^{-1}$ (Viveiros et al., 2010, 2020b). Even in grassland areas worldwide, the CO_2 production is usually lower than 50 g m^{-2} d^{-1} (Norman et al., 1992; Bajracharya et al., 2000; Nakadai et al., 2002). In addition, soil CO_2 fluxes measured in areas with similar vegetation and soil type located outside the anomalous zone did not exceed 34 g $m^{-2}d^{-1}$. Carbon isotopic data used in previous studies (Viveiros et al., 2020a; Viveiros et al., 2021) suggested a CO_2 biogenic background of 40 g m^{-2} d^{-1}. This observation again highlights the relevance of using carbon isotopic data to define the CO_2 sources, since the graphical statistical approach usually infers higher biogenic thresholds, as already showed in the literature (e.g., Chiodini et al., 2008; Viveiros et al., 2010, 2020b).

Spatial data were modeled with spherical variograms with different nuggets and ranges (Fig. 3). The CO_2 degassing map (Fig. 4a) shows that the highest flux areas are found close to the main visible degassing emissions. Diffuse Degassing Structures (DDS, Chiodini et al., 2001) cross these sites with similar and parallel NW-SE alignments, and are labeled as F1, 2, 3, 4, 5, 6 (Fig. 4a).

A positive spatial correlation is well observed between soil CO_2 flux and soil temperature. The highest correlation is established between the soil CO_2 flux and the air CO_2 concentration at 0.3 m above the ground (Fig. 4d; Table 4). Based on the soil CO_2 flux interpolated map a mean CO_2 release of ~40 t d^{-1} (±1.4 t d^{-1}) was estimated at Caldeiras da Ribeira Grande (area ~ 0.27 km^2), being ~30 t d^{-1} estimated as the deep-derived CO_2 (i.e., contribution above the chosen threshold, 40 g

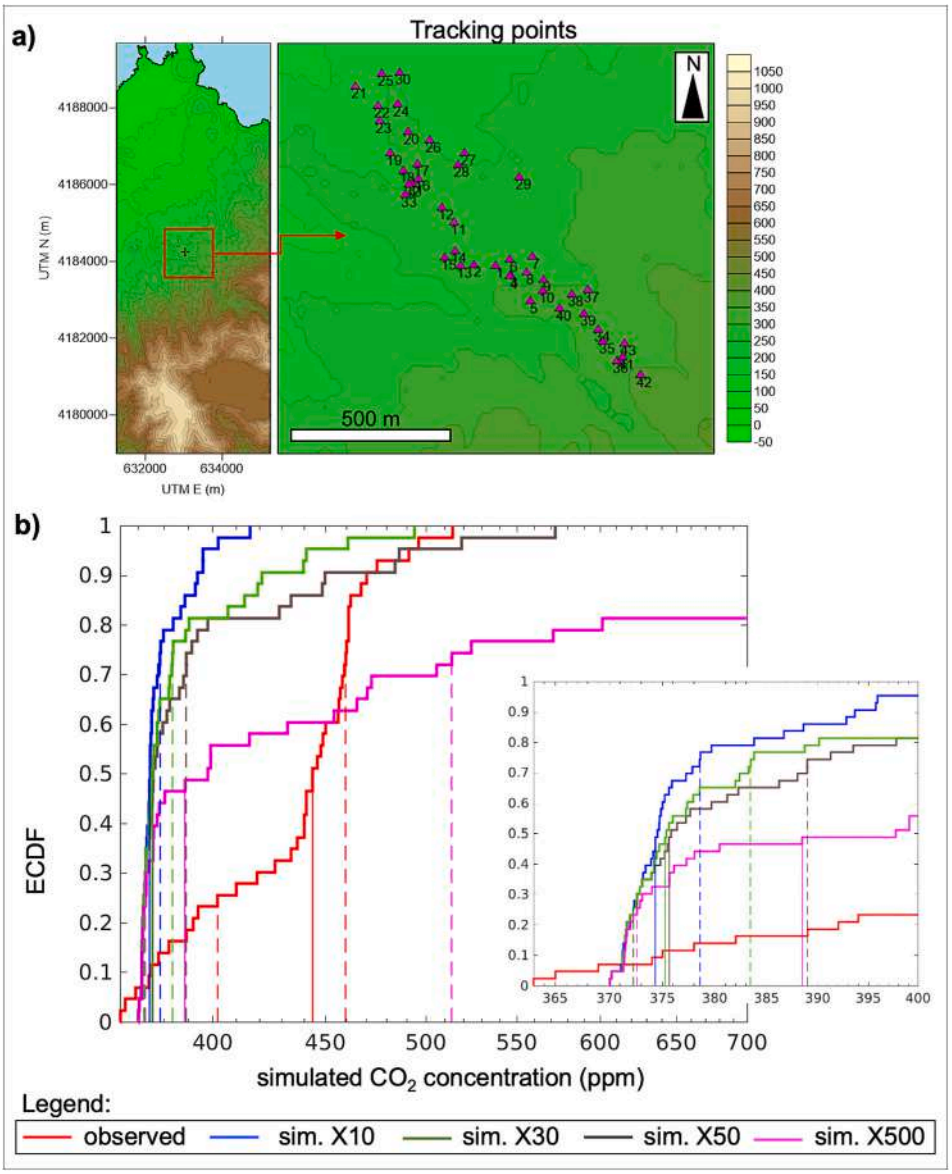

Fig. 5. a) Maps showing the investigated area (red box) with a magnification in which the tracking points are indicated as purple triangles; b) ECDFs of the observed (red curve) and simulated concentration values (other coloured curves) obtained by scaling the fumarolic flux with different scaling factors (*×10*, *×30*, *×50*, *×500*). The continuous vertical lines indicate the 50th percentile while the dashed lines indicate the 20th and 80th percentiles. (For interpretation of the references to colour in this figure legend, the reader is referred to the web version of this article.)

Table 2
- Descriptive statistics of soil CO_2 flux and concentrations, air and soil temperatures and barometric pressure of measured points.

Sampled variables	Number of measurements	Minimum	Maximum	Average	St. Dev.
Soil CO_2 flux (g $m^{-2}d^{-1}$)	830	6.55	5426	182	384
Soil temperature (°C)	830	20.8	80.7	30.7	8.3
Air temperature 0.30 m (°C)	830	18.6	37.1	25.1	2.9
Barometric pressure (mbar)	830	987	1000	993	4.0
CO_2 concentration 0.30 m (ppm)	830	330	1956	482	151
CO_2 concentration 1.50 m (ppm)	830	356	680	451	51

Table 3
Statistical parameters from the partitioned CO_2 flux populations and 90% confidence intervals of the mean at Caldeiras da Ribeira Grande.

Population	CO_2 source	proportion (%)	Mean CO_2 flux (g $m^{-2}d^{-1}$)	Mean CO_2 90% (confidence interval)
A	mainly biogenic	59	58.6	54.6–61.6
B	mainly volcanic - hydrothermal	41	377.4	316.7–470.1

$m^{-2}\,d^{-1}$). Considering that flux measurements were avoided close to the steam sites, this estimated CO_2 release corresponds to a minimum value for the diffuse emission only.

4.3. Model application

In this section, we describe the application of the gas dispersal model to Caldeiras da Ribeira Grande carried out using the results of soil CO_2 flux survey described in the Sections 4.1 and 4.2 as gas sources. We

Table 4
Pearson correlation coefficients for the variables measured in Caldeiras da Ribeira Grande during the fieldwork.

sampled variables	Soil temperature	Air temperature	Barometric pressure	Soil CO_2 flux	Air CO_2 concentration (0.30 m)	Air CO_2 concentration (1.50 m)
Soil temperature	1.00	0.36	0.10	0.32	0.32	−0.02
Air temperature	0.36	1.00	0.16	0.04	0.12	0.06
Soil CO_2 flux	0.32	0.04	0.10	1.00	0.47	0.05
CO_2 concentration (0.30 m)	0.32	0.12	0.07	0.47	1.00	0.29
CO_2 concentration (1.50 m)	−0.02	0.06	0.15	0.05	0.29	1.00

considered the available 43 tracking points over the investigated area: each one of them referred to a specific acquisition (in space and time) sampled during a selected day between 03/07/2021 and 03/08/2021 (Fig. 5a). The corresponding observed value is obtained by calculating the mean and the variance of all the available concentration measurements performed 30 min before and after the tracking point acquisition and within a 20 m radius (Table A2, Appendix A). The numerical dataset is obtained by simulating a continuous CO_2 dispersion from the source areas for the period from 03/07/2021 to 03/08/2021 (i.e., the time span for which we had available data) with meteorological conditions retrieved from the local weather station GFOG4. In the following, we present a statistical analysis on the model validation results, then we compare the observed and simulated data at 1.5 m from the ground corresponding to the 43 tracking points as reported in Figs. 5b. To do this, we followed the approach described in Massaro et al. (2021) by calculating the Empirical Cumulative Density Functions (ECDFs).

4.3.1. Statistical tests on model results

To test the goodness of fit between observations and model results which consider both diffuse and fumaroles contributions, the latter obtained with different scaling factors, we used the Aida indexes *K* and *k* (Aida, 1978) that measure the logarithmic distance between observed and simulated data. The Aida indexes, generally used for tsunamis and tephra dispersion problems (e.g., Kawamata et al., 2005; Poret et al., 2018), are defined as follow:

$$K = exp\left[\frac{1}{N}\sum_i^N log\left(\frac{x_{o,i}}{x_{s,i}}\right)\right] \tag{2}$$

$$k = exp\left\{\sqrt{\frac{1}{N}\sum_i^N log\left(\frac{x_{o,i}}{x_{s,i}}\right)^2 - \left[\frac{1}{N}\sum_i^N log\left(\frac{x_{o,i}}{x_{s,i}}\right)\right]^2}\right\} \tag{3}$$

A good fit between simulations and observed data is achieved when *K* is close to 1 (ideally $0.95 \leq K \leq 1.05$) and when *k* is minimized, with typical values <1.45 (Aida, 1978; Costa et al., 2014). Index *K* can be read as the mean scaling factor that should be applied to the simulated data to match the observed ones, while *k* represents the logarithmic mean dispersion between observed and simulated values.

It is worth noting that the calculation of the Aida indexes using all 43 selected tracking points provides an estimate of the global goodness of the fit but it does not give information on whether and which subset of the tracking points shows a better fit. Besides the analysis based on the Aida indexes, we provided further statistical parameters and tests (e.g., Morley et al., 2018). Regarding these tests, we calculated the Root Mean Square Error (RMSE):

$$RMSE = \sqrt{\frac{1}{N}\sum_i^N \left(x_{o,i} - x_{s,i}\right)^2} \tag{4}$$

where $x_{o,\,i}$, $x_{s,\,i}$ denote the observed and simulated values at tracking point *i* respectively, and *N* is the number of tracking points. The lower RMSE is, the closer are the simulated data to the observations.

We also calculated the Mean Bias Error (MBE) and the Relative Mean Bias Error (RMBE) in order to understand whether the simulated values tend to overestimate or underestimate the observations:

$$MBE = \frac{1}{N}\sum_i^N \left(x_{o,i} - x_{s,i}\right) \tag{5a}$$

$$RMBE = \frac{1}{N}\sum_i^N \frac{\left(x_{o,i} - x_{s,i}\right)}{x_{o,i}} \tag{5b}$$

Also in this case, the smaller the absolute value of MBE, the closer the simulated data are to the observed ones. The sign of MBE suggests whether the simulated values tend to overestimate (MBE > 0) or underestimate (MBE < 0) the observed ones. After that, we calculated the Mean Absolute Percentage Error (MAPE) as follow:

$$MAPE = \frac{100}{N}\sum_i^N \left|\frac{x_{o,i} - x_{s,i}}{x_{o,i}}\right| \tag{6}$$

By using these parameters, we carried out the bias histogram symmetry test to evaluate whether the simulated values have a systematic component. Completely random biases should have a gaussian distribution with zero mean. This test consists in building a histogram of the absolute biases, removing the values outside the 25th and 75th percentiles. If the histogram is not centered around 0 ppm, we can conclude that the simulated data are systematically over/underestimating the measured ones. To do this, we calculated the Inter-Quartile Range (IQR) as:

$$IQR = H_{max} - H_{min} \tag{7}$$

where H_{max}, H_{min} are the values of the upper edge of the maximum bin and the lower edge of the minimum bin of the bias histogram, respectively. The value of IQR gives a measure of how much the biases are spread, so the lower it is, the closer the simulated values are to the observed ones. In Appendix (Fig. A2) we reported the IQR histograms for the different fumarolic scaling factors. The results of all these parameters and tests are summarized in Table 5 (Aida indexes *K* and *k*, RMSE, MBE, MAPE, and IQR).

We found that the ×30 scaling has the best performance in estimating the fumarolic flux, as it produces the lowest MAPE and RMSE, whereas the case ×150 is better to minimize the biases. Moreover, the smallest Aida's index *k* is obtained for the cases ×10 and ×30 although the corresponding *K* indicate a larger estimate of the overall gas fluxes of about 10%.

The differences observed in the statistical indicators (Table 5) highlight the fact that we cannot minimize both the errors and the

Table 5
Estimates of the statistical parameters and tests calculated to compare simulated and observed data for each degassing scenario scaled with different scaling factors (*×10, ×30, ×50, ×100, ×150, ×250, ×500, ×1000*). *K*, *k*, RMSE, MBE, RMBE, MAPE, and IQR (see Eqs. 2–7).

Scaling factors	K	k	RMSE (ppm)	MBE (ppm)	RMBE	MAPE (%)	IQR
×10	1.14	1.09	66.69	−55.01	0.12	12.90	52.27
×30	1.12	1.11	63.66	−46.08	0.10	11.88	64.95
×50	1.09	1.13	66.38	−37.16	0.08	12.13	75.55
×100	1.05	1.20	92.93	−14.90	0.03	15.49	85.18
×150	1.01	1.27	132.69	7.35	−0.02	19.54	89.86
×250	0.95	1.39	223.42	51.89	−0.12	28.35	121.26
×500	0.85	1.63	463.07	163.37	−0.38	52.35	197.03
×1000	0.72	1.98	949.53	386.31	−0.89	101.73	320.99

biases.

4.3.2. Empirical Cumulative Density Functions (ECDFs)

For each tracking point (Fig. 5a), we compared the observed CO_2 concentration at a reference height (1.5 m from the ground) and the simulated one. This comparison refers to the diffuse CO_2 flux measured during the survey.

Since the fumarolic flux that would be added to the diffuse one is unknown (because of the limit of the accumulation chamber method), we used the diffuse flux measured in positions as close as possible to the fumaroles as reference values to be scaled.

In Fig. 5b we reported the ECDFs of the simulated CO_2 concentration obtained by using the diffusive flux in the entire domain and adding the scaled fumarolic flux where the fumaroles are located. Each ECDF collects the observed (red curve) and simulated CO_2 concentration of the entire tracking points dataset (43) obtained by using different scaling factors (Table 5). For simplicity, only the results with scaling factors of $\times$10, $\times$30, $\times$50, $\times$500 are shown.

Inspecting how far apart are the means (solid lines) of the distribution and the 20th and 80th percentiles (dotted lines), we note the effect of the scaling that splits the upper part of the simulated ECDFs corresponding to those tracking points closest to fumaroles (Fig. 1c) that show higher CO_2 concentrations (>50 ppm above the background level). On the contrary, the scaling factors have a negligible influence on the further tracking points, which are mainly influenced by the diffuse contribution, with lower concentration (~ <50 ppm above the background level).

From such a plot it is possible to see the best agreement by visualizing which case can overlap or is closer to the curve representing the observations. Moreover, by considering the statistical analysis on model results, the scaling $\times$30 has the best performance in estimating the fumarolic flux, taking into account the increase of 10%, due to the fact that the Aida index K returned 1.12, that is about 10%.

In this light, we find that the total scaled flux corresponds to ~209 t d^{-1}. Such an estimate is composed of ~174 t d^{-1} as fumarolic and ~ 35 t d^{-1} as diffuse contribution. This latter is in good agreement with the reference value of 40 t d^{-1} obtained by the gas survey.

4.4. Probabilistic CO_2 concentration maps

To build the long-term probabilistic concentration maps of the CO_2 dispersion at Caldeiras da Ribeira Grande, a robust statistical variability of wind conditions is needed. To do this, reanalysis data were randomly sampled from the ECMWF ERA5 database (https://www.ecmwf.int/en/forecasts/datasets/reanalysis-datasets/era5; Climate Change Service, 2017) considering an ensemble of 1000 days over the last 30 years (from 01/01/1991 to 31/12/2020). As reported in Section 4.3, the selected gas flux scenario was built using the fumarolic contribution scaled by $\times$30 since it is the best result of the model validation.

Basically, the probabilistic concentration maps show the value of CO_2 concentration (in ppm) that can be overcome of an exceedance probability p (i.e., within the timespan of a day there is a probability p that the CO_2 concentration in the specific point will be greater than the displayed value). In Fig. 6, we show the concentration maps referring to the last timestep of each day (23:00) at 0.30 m (height representative for small animals) and 1.50 m (height representative for human breath)

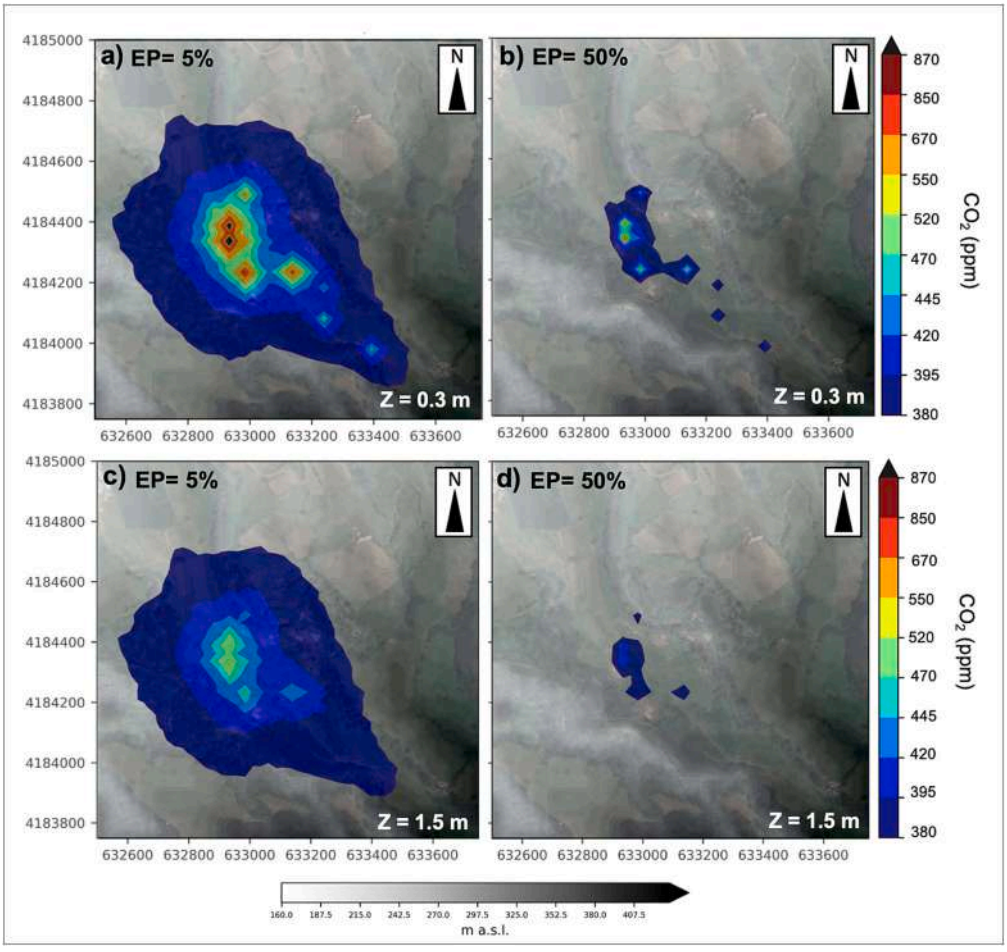

Fig. 6. Long-term probabilistic CO_2 concentration maps show the exceedance probability (EP) of 5% and 50% at two different atmospheric levels: a-b) 0.30 m and c-d) 1.5 m from the ground. Superimposed to the grayscale representation of the topography (DEM courtesy the SIG team, IVAR).

from the ground, at the 5% and 50% exceedance probability. In Fig. 6a, the 5% exceedance probability concentration map at 0.30 m displays greater values of CO_2 concentration, locally reaching maximum peaks of ~1075 ppm (considering the background level of ~370 ppm) that decrease to ~530 ppm in the 50% exceedance probability map (Fig. 6b). The 5% exceedance probability map at 1.50 m (Fig. 6c) shows peaks of CO_2 concentration of ~602 ppm that became slightly lower (~418 ppm) at 50% exceedance probability (Fig. 6d). These results are in good accordance with the averaged observed data reported in Table 2 (i.e., 482, 451 ppm).

5. Discussion

The Caldeiras da Ribeira Grande degassing area has been expanded since 2010 around pre-existing fumaroles (F1 in Fig. 1C). In this study, an emission of ~40 t d^{-1} was preliminarily estimated for the diffuse degassing during July/August 2021 from an area of about 0.27 km^2, showing that the most of the CO_2 (30 t d^{-1}) has a volcanic-hydrothermal origin. This is the minimum value estimated for the CO_2 fluxes emitted in the area since sampling was avoided in the steam emission sites. Consequently, the fumarolic flux contribution in these areas was not accounted for.

CO_2 spatial distribution showed that the larger anomaly area is located inside the river that crosses the area, including the dismissed geothermal well, where hydrothermal activity is clearly visible (F3 and F4 in Fig. 1C). These areas also overlap with the identified thermal anomalies (Fig. 4B). Grassland dominates the sampled area and the lowest soil CO_2 flux values (corresponding to population A, Table 3) probably result from the soil respiration in these areas. Close to the main fumaroles, especially in the pre-existing fumarolic field (F1 in Fig. 1c), some low CO_2 fluxes may result from impermeable soil layers due to clayey alteration in the area (Mateus et al., 2015). As known, CO_2 degassing occurs as permanent manifestations or as episodic phenomena and may be affected by local topography, meteorology, surface roughness and/or atmospheric stability (Oliveira et al., 2018; Rinaldi et al., 2012; Viveiros et al., 2009, 2015a).

The DDS defined in the sampled area (Fig. 4a) show a general NW-SE direction, similar to the alignments previously inferred for the area by Carmo et al. (2015). Tectonic structures were not previously mapped at Caldeiras da Ribeira Grande, probably due to the existing vegetation together with the thick pumice deposits that hide eventual structures (Carmo et al., 2015). However, the consistent lineaments of gas anomalies observed in the current study suggest a deep structural control for the gas emission and the existence of hidden tectonic structures in the study area.

In what concerns gas dispersion, in the current study we noted that higher CO_2 concentrations were measured close to the soil, as it would be expected considering the CO_2 origin (Fig. 4D; Fig. 7A).

The model validation was able to indicate the best fit scaling factor (×30 increased by 10%; Fig. 5b) to apply at the diffuse gas fluxes close to the fumarolic sources whose flux is unknown. In this way, the total amount of gas flux emitted by soil and fumaroles can be inferred in the investigated area.

The simulated diffuse contribution of ~35 t d^{-1} shows a full agreement with observations (~40 t d^{-1}). Moreover, the estimated fumarolic contribution is of ~174 t d^{-1} (Table 5).

Aiuppa et al. (2020) observed similar predominance of the fumarolic CO_2 over the soil diffuse degassing for the crater fumaroles of Fogo Volcano (Cape Verde). Werner et al. (2000) also estimated that the Mud Volcano vent emissions (Yellowstone, USA) contributed to >32% of the total degassing. Contrarily, at Campi Flegrei, the diffuse degassing dominates (usually >1000 t d^{-1}) over the fumarolic emissions (see Fig. 7 of Cardellini et al., 2017). Fridriksson et al. (2006) at Reykjanes area (Iceland) also showed that the soil CO_2 diffuse degassing corresponds to about 97% of the total CO_2 emission.

Pedone et al. (2015) highlighted that when one considers the large

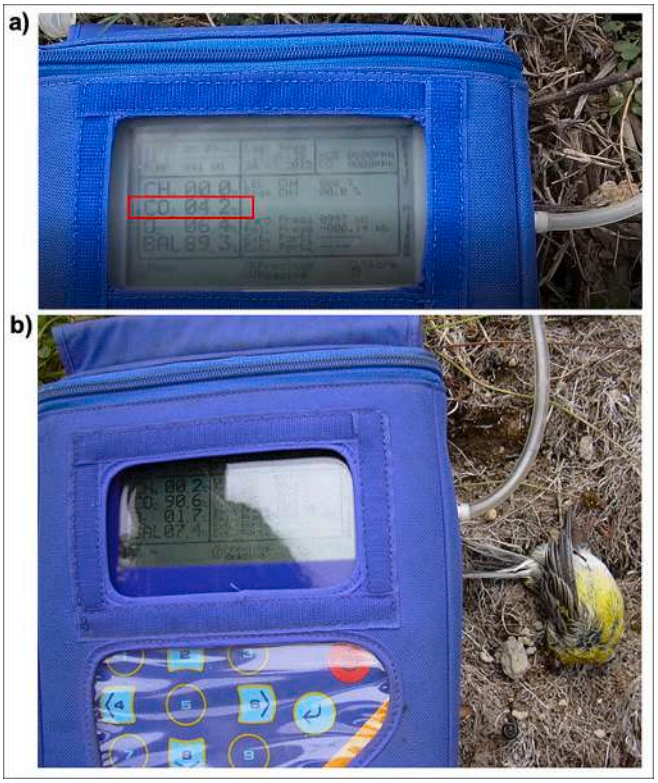

Fig. 7. a) Photo showing a high CO_2 concentration (42,000 ppm) measured on the ground during the 2021 fieldwork; b) Detail of a little dead bird found in the area. Photo by Fátima Viveiros.

Furnas volcanic system (caldera and south flank), the diffuse degassing CO_2 (Viveiros et al., 2010) dominates over the estimation of the fumarolic emission. However, at the scale of fumarolic ground, the estimated fumarolic contribution was higher than the diffuse degassing. Additional studies are lacking in the literature that couple diffuse degassing and fumarolic emissions estimations. Nevertheless, this study again highlights the contribution of the permanent gas emissions (diffuse degassing and fumarolic processes) to evaluate the global volcano carbon budget, as recently shown in the literature (Werner et al., 2019; Fischer and Aiuppa, 2020).

Previous studies recognized visible manifestations of volcanism at Fogo Volcano (Viveiros et al., 2015a, 2015b) and diffuse degassing from soil (Viveiros et al., 2015b) and lake (Andrade et al., 2020) areas were also mapped (in particular, at Fogo Lake, CO_2 originated from a biogenic source). An interesting comparison can be done between the gas flux estimated in this study with several areas of the Azores archipelago standardized by area (Table 6). For instance, we note that the hydrothermal CO_2 released at Caldeiras da Ribeira Grande is of the same order of magnitude of the CO_2 emitted at Furnas Volcano (Viveiros et al., 2010, 2012) and Furnas do Enxofre fumarolic field (Viveiros et al., 2020a).

From a hazard perspective, our model results did not show CO_2 concentrations above the minimum hazard threshold of 5,000 ppm (e.g., NIOSH, 2007; Granieri et al., 2013; Viveiros et al., 2016) at any of the two simulated heights, although hazardous indoor CO_2 concentrations were locally measured in the Caldeiras da Ribeira Grande buildings (Viveiros et al., 2021) as well as close to the soil (at the ground level or even in depressions/confined spaces) as shown in Fig. 7a. In fact, the accumulation of hazardous concentrations close to the soil dilutes when the gas is measured and simulated at 30 cm height. Previous studies (Viveiros et al., 2008, 2009, 2015b) showed seasonal trends on the soil CO_2 emissions with higher fluxes being measured in the winter period. Additional studies are thus suggested to be carried out in the winter

Table 6
Soil CO_2 emissions at the Azores archipelago degassing sites sorted by area.

Island	Volcanic System	Sampled site	Soil diffuse CO_2			References
			Hydrothermal emission (t d^{-1})	Sampled area (km^2)	CO_2/area (t d^{-1} km^{-2})	
S. Miguel	Furnas	Furnas Volcano	945	6.2	152	Viveiros et al. (2012)
S. Miguel	Fogo	Caldeiras da Ribeira Grande	30	0.27	111	Current study
Terceira	Pico Alto	Furnas do Enxofre	2.54	0.024	106	Viveiros et al. (2020b)
S.Miguel	Sete Cidades	Ferraria	5.23	0.47	11	Lisetti (2013)

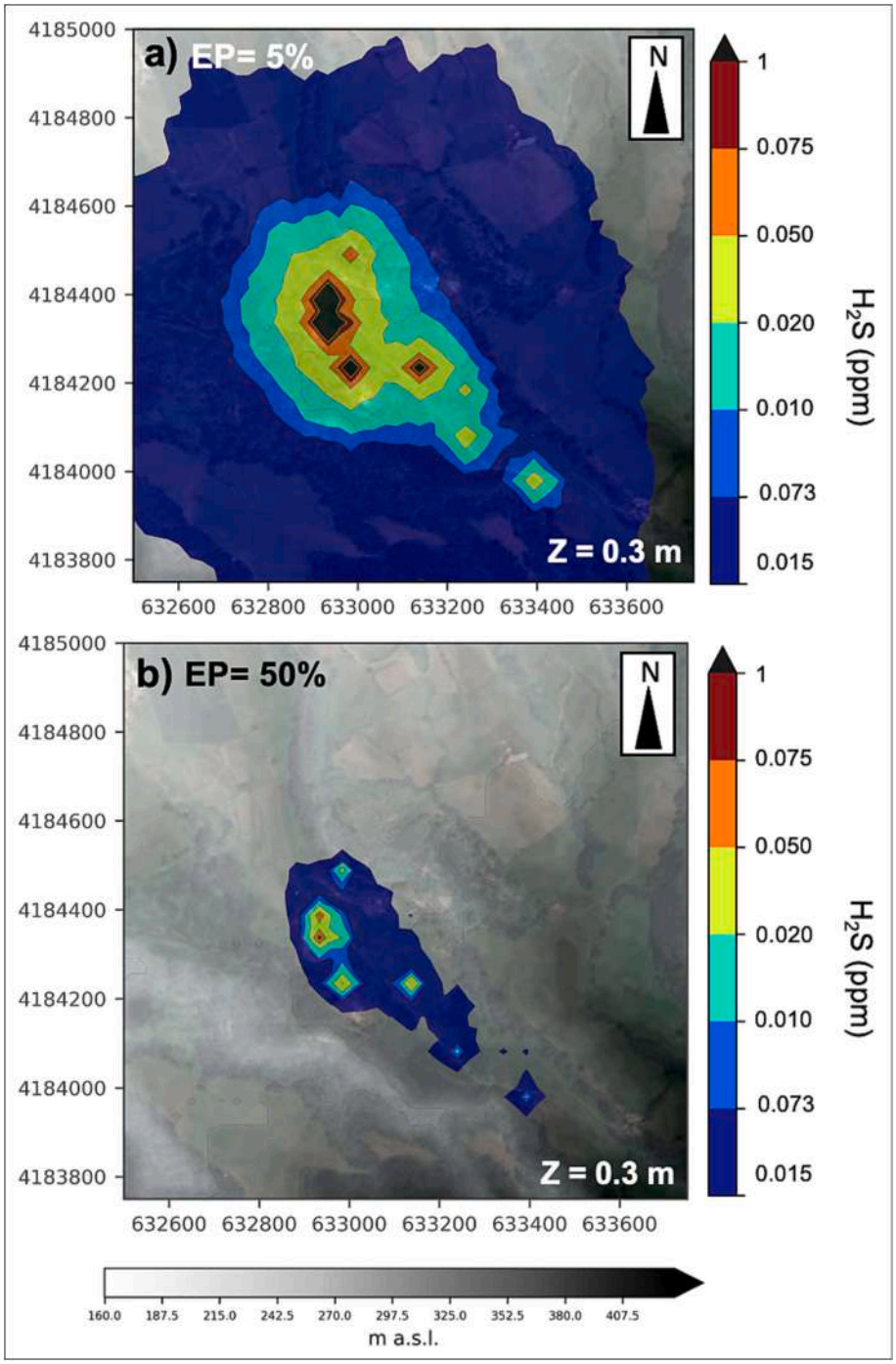

Fig. 8. Long-term probabilistic H_2S concentration maps obtained by scaling ×50 the fumarolic flux, considering a meteorological variability over the last 30 years (1991–2020). The maps show the exceedance probability (EP) of a) 5% and b) 50% at 0.3 m from the ground. Superimposed to the grayscale representation of the topography (DEM courtesy the SIG team, IVAR).

season to evaluate potential variations on the dispersion results and main outputs estimated.

Moreover, we cannot also exclude the potential impact of the H_2S in the gas plume. Although there are no robust indications of lethal dose for small animals in the literature (data are mainly provided for rats, e.g., Moulin et al., 2022; Dorman et al., 2004), we know that the exposure to low H_2S concentration can be harmful for humans (in the range of 0.015–0.15 ppm; e.g., Settimo et al., 2016) and very likely also for small animals (see Fig. 7b). For this reason, we also provided the long-term probabilistic concentration maps for H_2S cautiously based on the highest H_2S/CO_2 molar ratio measured in the investigated area (Fig. 8). In this case, the simulated CO_2 concentrations (Fig. 6) were converted in H_2S by using a representative H_2S/CO_2 molar ratio of 3×10^{-3} (as reported in Caliro et al., 2015, in accordance with the highest measurement of the molar ratios acquired in their survey). Here we only focused the attention on a height of 0.30 m from the ground showing that some of the thresholds considered relevant for human health were overcome at 5% and 50% exceedance probabilities (for example, 0.015 ppm: tolerable range of concentrations for short period, 30 min; 0.11 ppm: daily averaged threshold; 0.15 ppm: paralysis of optic nerve; 500 ppm death after few minutes; Settimo et al., 2016). In particular, the peaks reached in these maps are ~2.7 ppm (at 5% exceedance probability) and ~ 0.9 ppm (at 50% exceedance probability).

6. Conclusions

In this work, we presented the results of a survey carried out during July/August 2021 aimed to estimate the gas fluxes at Caldeiras da Ribeira Grande. Soil CO_2 fluxes were quantified through field campaigns and a minimum diffuse flux of ~40 t d^{-1} was estimated. Two populations for the CO_2 released were found, highlighting biogenic and volcanic-hydrothermal sources.

Beyond the use of degassing maps to contribute to the estimation of the global carbon budget and to identify hidden tectonic structures, this study offers, for the first time, the indirect estimation of the fumarolic flux (~174 t d^{-1}) through a statistical model validation able to find out a best fit between observed and simulated CO_2 concentrations. Such a validation allowed us to provide the estimate of the diffuse CO_2 flux (~35 t d^{-1}), in good accordance with the field data. As in this new modeling there is a good agreement between the values measured in situ and the simulations, we highlight the potential to use this method to estimate total fluxes in other hydrothermal areas, where there is difficulties in estimate the hydrothermal fluxes, and this is quite important for the estimation of the carbon budget.

Moreover, the long-term probabilistic concentration maps of CO_2 revealed that no hazardous thresholds for humans can be reached at 5% and 50% exceedance probability, considering the present-day gas dispersal scenario. However, the death of small animals may be both due to local CO_2 concentration that occasionally reached peaks in poorly ventilated areas or depression, and to the presence of H_2S. By using the highest H_2S/CO_2 measured molar ratio in the area as reference, we converted the simulated CO_2 concentrations in H_2S values showing that peaks of ~2 and ~ 1 ppm could be reached at 0.3 m from the ground, considering the 5% and 50% exceedance probability, respectively.

Supplementary data to this article can be found online at https://doi.org/10.1016/j.jvolgeores.2023.107807.

Funding

The research was supported by the MAGAT project (FCT funded, Ref. CIRCNA/OCT/2016/2019). EB was supported by a Ph.D. grant from Fundação para a Ciência e Tecnologias (FCT, Portuguese Government, Ref. UI/BD/150921/2021). MS was supported by the CIR01_00013 PON-GRINT Project. Also, this research was partially supported by MIUR, grant number project no. PRIN2017-2017LMNLAW "Connect4Carbon".

CRediT authorship contribution statement

Fátima Viveiros: Project administration, Supervision, Conceptualization, Investigation, Methodology, Software, Validation, Formal analysis, Data curation, Visualization, Writing – original draft, Writing – review & editing. **Eleonora Baldoni:** Investigation, Methodology, Software, Data curation. **Silvia Massaro:** Conceptualization, Investigation, Methodology, Validation, Formal analysis, Writing – original draft, Writing – review & editing. **Manuel Stocchi:** Conceptualization, Investigation, Methodology, Validation, Formal analysis, Writing – review & editing. **Antonio Costa:** Conceptualization, Investigation, Methodology, Validation, Formal analysis, Writing – review & editing. **Stefano Caliro:** Conceptualization, Investigation, Methodology, Resources, Data curation. **Giovanni Chiodini:** Conceptualization, Investigation, Methodology, Resources, Data curation. **César Andrade:** Conceptualization, Investigation, Methodology, Resources, Data curation.

Declaration of Competing Interest

The authors declare that they have no known competing financial interests or personal relationships that could have appeared to influence the work reported in this paper.

Data availability

Datasets related to this article can be found in Appendix A.

Acknowledgments

The authors thank Rui Mestre, Vanessa Soares and Dee Cirium for the help with the soil degassing surveys, and Lucia Moreno for the calibration of the portable flux meters. The topography used is a courtesy SIG team, IVAR/CIVISA. We warmly thank Jacopo Selva for his advice in statistical tests.

References

Aida, I., 1978. Reliability of a tsunami source model derived from fault parameters. J. Phys. Earth 26 (1), 57–73. https://doi.org/10.4294/jpe1952.26.57.

Aiuppa, A., Bitetto, M., Rizzo, A.L., Viveiros, F., Allard, P., Frezzotti, M.L., Valenti, V., Zanon, V., 2020. The fumarolic CO_2 output from Pico do Fogo Volcano (Cape Verde). Ital. J. Geosci. 139, 325–340.

Allard, P., Carbonnelle, J., Dajlevic, D., Le Bronec, J., Morel, P., Robe, M.C., Maurenas, J. M., Faivre-Pierret, R., Martin, D., Sabroux, J.C., Zettwoog, P., 1991. Eruptive and diffuse emissions of CO_2 from Mount Etna. Nature 351, 387–391.

Andrade, C., Viveiros, F., Cruz, J.V., Coutinho, R., Silva, C., 2016. Estimation of the CO_2 flux from Furnas volcanic Lake (São Miguel, Azores). J. Volcanol. Geotherm. Res. 315, 51–64.

Andrade, C., Cruz, J.V., Viveiros, F., Coutinho, R., 2020. CO_2 emissions from Fogo intra caldera volcanic lakes (São Miguel Island, Açores): a tool for volcanic monitoring. J. Volcanol. Geotherm. Res. 400, 106915 https://doi.org/10.1016/j.jvolgeores.2020.106915.

Andrade, C., Cruz, J.V., Viveiros, F., Coutinho, R., 2021. Diffuse CO_2 emissions from Sete Cidades volcanic lake (São Miguel Island, Azores): influence of eutrophication processes. Environ. Pollut. 268, 115624.

Bajracharya, R.M., Lal, R., Kimble, J.M., 2000. Diurnal and seasonal CO2-C flux from soil as related to erosion phases in Central Ohio. Soil Sci. Soc. Am. J. 64, 286–293.

Barberi, F., Carapezza, M.L., Ranaldi, M., Tarchini, L., 2007. Gas blowout from shallow boreholes at Fiumicino (Rome): induced hazard and evidence of deep CO_2 degassing on the Tyrrhenian margin of Central Italy. J. Volcanol. Geotherm. Res. 165, 17–31.

Barberi, F., Carapezza, M.L., Tarchini, L., Ranaldi, M., Ricci, T., Gattuso, A., 2019. Anomalous Discharge of Endogenous Gas at Lavinio (Rome, Italy) and the Lethal Accident of 5 September 2011. GeoHealth 3, 407–422. https://doi.org/10.1029/2019GH000211.

Beaubien, S.E., Ciotoli, G., Lombardi, S., 2003. Carbon dioxide and radon gas hazard in the Alban Hills area (Central Italy). J. Volcanol. Geotherm. Res. 123, 63–80.

Bergfeld, D., Goff, F., Allard, P., 2001. High CO_2 flux measurements in volcanic and geothermal areas, methodologies and results. Chem. Geol. 177.

Bettencourt, M.L., 1979. O clima dos Açores como recurso natural na aplicação especialmente em agricultura e indústria do turismo. Lisboa, Instituto Nacional de Meteorologia e Geofísica (in Portuguese).

Biagi, R., Tassi, F., Caliro, S., Capecchiacci, F., Venturi, S., 2022. Impact on air quality of carbon and sulfur volatile compounds emitted from hydrothermal discharges: the

case study of Pisciarelli (Campi Flegrei, South Italy). Chemosphere 297. ISSN 0045-6535. https://doi.org/10.1016/j.chemosphere.2022.134166. ISSN 0045-6535.
Blong, R.J., 1984. Volcanic Hazards. A Sourcebook on the Effects of Eruptions. Academic Press, London.
Brombach, T., Hunziker, J., Chiodini, G., Cardellini, C., Marini, L., 2001. Soil diffuse degassing and thermal energy fluxes from the southern Lakki plain, Nisyros (Greece). Geophys. Res. Lett. 28 (1), 69–72.
Caliro, S., Viveiros, F., Chiodini, G., Ferreira, T., 2015. Gas geochemistry of hydrothermal fluids of the S. Miguel and Terceira Islands, Azores. Geochim. Cosmochim. Acta 168, 43–57.
Carapezza, M.L., Granieri, D., 2004. CO_2 soil flux at Vulcano (Italy): comparison between active and passive methods. Appl. Geochem. 19, 73–88.
Carapezza, M.L., Tarchini, L., Ancona, C., Forastiere, F., Ranaldi, M., Ricci, T., De Simone, G., Mataloni, F., Pagliuca, N.M., Barberi, F., 2022. Health impact of natural gas emission at Cava dei Selci residential zona (metropolitan city of Rome, Italy). Environ. Geochem. Health. https://doi.org/10.1007/s10653-022-01244-6.
Cardellini, C., Chiodini, G., Frondini, F., 2003. Application of stochastic simulation to CO2 flux from soil: mapping and quantification of gas release. J. Geophys. Res. 108 (B9), 2425. https://doi.org/10.1029/2002JB002165-.
Cardellini, C., Chiodini, G., Frondini, F., Avino, R., Bagnato, E., Caliro, S., Lelli, M., Rosiello, A., 2017. Monitoring diffuse volcanic degassing during volcanic unrests: the case of Campi Flegrei (Italy). Sci. Rep. 7 (1), 1–15.
Carmo, R., Madeira, J., Ferreira, T., Queiroz, G., Hipólito, A., 2015. Volcano tectonic structures of São Miguel Island, Azores. Geol. Soc. Lond. Mem. 44, 65–86. https://doi.org/10.1144/M44.6.
Chiodini, G., Frondini, F., Raco, B., 1996. Diffuse emission of CO2 from the Fossa crater, Vulcano Island (Italy). Bull. Volcanol. 58 (1), 41–50.
Chiodini, G., Cioni, R., Guidi, M., Raco, B., Marini, L., 1998. Soil CO2 flux measurements in volcanic and geothermal areas. Appl. Geochem. 13, 543–552.
Chiodini, G., Frondini, F., Cardellini, C., Granieri, D., Marini, L., Ventura, G., 2001. CO2 degassing and energy release at Solfatara volcano, Campi Flegrei, Italy. J. Geophys. Res. 106 (B8), 16, 213–16, 221.
Chiodini, G., Caliro, S., Cardellini, C., Avino, R., Granieri, D., Schmidt, A., 2008. Carbon isotopic composition of soil CO2 efflux, a powerful method to discriminate different sources feeding soil CO2 degassing in volcanic-hydrothermal areas. Earth Planet. Sci. Lett. 274, 372–379.
Cortis, A., Oldenburg, C.M., 2009. Short-range atmospheric dispersion of carbon dioxide. Boundary-Layer. Meteorol. 133 (1), 17–34.
Costa, A., Chiodini, G., 2015. Modelling air dispersion of CO_2 from limnic eruptions. In: Volcanic Lakes. Springer, Berlin, Heidelberg, pp. 451–465.
Costa, A., Macedonio, G., 2016. DISGAS: A Model for Passive DISpersion of GAS. Rapporti tecnici INGV. 332. Istituto Nazionale Di Geofisica e Vulcanologia, Italy (2039e7941).
Costa, A., Macedonio, G., Chiodini, G., 2005. Numerical model of gas dispersion emitted from volcanic sources. Ann. Geophys. 48 (4–5).
Costa, A., Folch, A., Macedonio, G., 2013. Density-driven transport in the umbrella region of volcanic clouds: Implications for tephra dispersion models. Geophys. Res. Lett. 40 (18), 4823–4827.
Costa, A., Smith, V.C., Macedonio, G., Matthews, N.E., 2014. The magnitude and impact of the Youngest Toba Tuff super-eruption. Front. Earth Sci. 2, 16.
Cruz, J.V., França, Z., 2006. Hydrogeochemistry of thermal and mineral springs of the Azores archipelago (Portugal). J. Volcanol. Geotherm. Res. 151, 382–398.
Deutsch, C.V., Journel, A.G., 1998. GSLIB: Geostatistical Software Library and User's Guide. Appl. Geostat. Ser. 369. Oxford Univ. Press, N. Y.
Dioguardi, F., Massaro, S., Costa, A., Chiodini, G., Folch, A., Macedonio, G., Sandri, L., Selva, J., Tamburello, G., 2022. VIGIL: a python tool for automatized probabilistic Volcanic Gas dIspersion modelLing. Ann. Geophys. 65 (1), DM107. https://doi.org/10.4401/ag-8796.
Dorman, D.C., Struve, M.F., Gross, E.A., 2004. Respiratory tract toxicity of inhaled hydrogen sulfide in Fischer-344 rats, Sprague-Dawley rats, and B6C3F1 mice following subchronic (90-day) exposure. Toxicol. Appl. Pharmacol. 198, 29–39.
Douglas, S.G., Kessler, R.C., Carr, E.L., 1990. User's Guide for the Urban Airshed Model. Volume 3. User's manual for the Diagnostic Wind Model (No. PB-91-131243/XAB). Systems Applications, Inc., San Rafael, CA (USA).
Fischer, T.P., Aiuppa, A., 2020. AGU Centennial Grand Challenge: Volcanoes and deep carbon global CO2 emissions from subaerial volcanism - recent progress and future challenges. Geochem. Geophys. Geosyst. 21 https://doi.org/10.1029/2019GC008690 e2019GC008690.
Folch, A., Costa, A., Hankin, R.K.S., 2009. TWODEE-2: a shallow layer model for dense gas dispersion on complex topography. Comput. Geosci. 35, 667–674. https://doi.org/10.1016/j.cageo.2007.12.017.
Folch, A., Barcons, J., Kozono, T., Costa, A., 2017. High-resolution modeling of atmospheric dispersion of dense gas using TWODEE-2.1: application to the 1986 Lake Nyos limnic eruption. Nat. Hazards Earth Syst. Sci. 17, 1–19. https://doi.org/10.5194/nhess-17-861-2017.
Fridriksson, T., Kristjánsson, B.R., Ármannsson, H., Margrétardóttir, E., Ólafsdóttir, S., Chiodini, G., 2006. CO_2 emissions and heat flow through soil, fumaroles, and steam heated mud pools at the Reykjanes geothermal area, SW Iceland. Appl. Geochem. 21, 1551–1569.
Gaspar, J.L., Ferreira, T., Queiroz, G., Baubron, J.C., Baxter, P., 1998. High Levels of CO2 in the Atmosphere of Furna do Enxofre Lava Cave (Graciosa Island, Azores): a Case of Public Health Risk. EC Advanced Study Course 1998. Volcanic Hazard Assessment, Monitoring and Risk Mitigation. European Commission, Environment and Climate Programme (abstract), p. 70.
Gaspar, J.L., Queiroz, G., Ferreira, T., Medeiros, A.R., Goulart, C., Medeiros, J., 2015. Earthquakes and volcanic eruptions in the Azores region: geodynamic implications from major historical events and instrumental seismicity. In: Gaspar, J.L., Guest, J.E., Duncan, A.M., Barriga, F.J., Chester, D.K. (Eds.), Volcanic Geology of São Miguel Island (Azores Archipelago), vol. 44. Geol. Soc., London Mem., pp. 33–49
Goovaerts, P., 1999. Geostatistics in soil science: state-of-the-art and perspectives. Geoderma 89, 1–45. https://doi.org/10.1016/S0016-7061(98)00078-0.
Granieri, D., Costa, A., Macedonio, G., Bisson, M., Chiodini, G., 2013. Carbon dioxide in the urban area of Naples: Contribution and effects of the volcanic source. J. Volcanol. Geotherm. Res. 52-61 https://doi.org/10.1016/j.jvolgeores.2013.05.003.
Hankin, R.K.S., Britter, R.E., 1999. Twodee: the Health and Safety Laboratory's shallow layer model for heavy gas dispersion part 3: Experimental validation (Thorney Island). J. Hazard. Mater. 66 (3), 239–261.
Hersbach, H., Bell, B., Berrisford, P., Biavati, G., Horányi, A., Muñoz Sabater, J., Nicolas, J., Peubey, C., Radu, R., Rozum, I., Schepers, D., Simmons, A., Soci, C., Dee, D., Thépaut, J-N. (2018). ERA5 hourly data on single levels from 1940 to present. Copernicus Climate Change Service (C3S) Climate Data Store (CDS). 10.24381/cds.adbb2d47, (Accessed on 07-MAR-2023).
Kawamata, K., Takaoka, K., Ban, K., Imamura, F., Yamaki, S., Kobayashi, E., 2005. Model of tsunami generation by collapse of volcanic eruption: The 1741 Oshima-Oshima tsunami. In: Tsunamis. Springer, Dordrecht, pp. 79–96.
Le Guern, F., Tazieff, H., Faivre-Pierret, R., 1982. An example of health hazard: people killed by gas during a phreatic eruption: Dieng Plateau (Java, Indonesia), February 20th 1979. Bull. Volcanol. 45, 153–156.
Lisetti, A., 2013. Studio del flusso di CO2 diffuso dal suolo nell'area di ponta da Ferraria, são Miguel, Azzorre. Masther Thesis. Università degli Studi di Perugia, Italy.
Marques, R., Zêzere, J., Trigo, R., Gaspar, J., Trigo, I., 2007. Rainfall patterns and critical values associated with landslides in Povoação County (São Miguel Island, Azores): relationships with the North Atlantic Oscillation. Hydrol. Process. 22 https://doi.org/10.1002/hyp.6879:478-494.
Massaro, S., Dioguardi, F., Sandri, L., Tamburello, G., Selva, J., Moune, S., Jessop, D.E., Moretti, R., Komorowski, J.-C., Costa, A., 2021. Testing gas dispersion modelling: a case study at La Soufrière volcano (Guadeloupe, Lesser Antilles). J. Volcanol. Geotherm. Res. 417 https://doi.org/10.1016/j.jvolgeores.2021.107312.
Massaro, S., Stocchi, M., Tamburello, G., Costa, A., Sandri, L., Caliro, S., Chiodini, G., Selva, J., Dioguardi, F., Folch, A., 2022. Validating gas dispersion modelling at La Solfatara (Campi Flegrei, South Italy). Nuovo Cimento Soc. Ital. Fis. C 45 (6), 186.
Mateus, A., Carvalho, M.R., Nunes, J.C., Carvalho, J.M., 2015. Influence of wall-rock alteration and fluid mixing mechanisms in the chemistry of thermal fluids and mud-pool sediments at Caldeiras da Ribeira Grande (S. Miguel Island, Azores). Environ. Earth Sci. 73, 2809–2831. https://doi.org/10.1007/s12665-014-3439-7.
Morley, S.K., Brito, T.V., Welling, D.T., 2018. Measures of model performance based on the log accuracy ratio. Space Weather 16, 69–88. https://doi.org/10.1002/2017SW001669.
Moulin, F.J.-M., Brenneman, K.A., Kimbell, J., Dorman, D.C., 2022. Predicted regional flux of hydrogen sulfide correlates with distribution of nasal olfactory lesions in rats. Toxicol. 66, 7–15.
Nakadai, T., Yokozawa, M., Ikeda, H., Koizumi, H., 2002. Diurnal changes of carbon dioxide flux from bare soil in agricultural field in Japan. Appl. Soil Ecol. 19, 161–171.
NIOSH, 2007. Niosh Pocket Guide to Chemical Hazards. DHHS (NIOSH) Publication, No. 2005–149. US Government Printing Office, Washington DC.
Norman, J.M., Garcia, R., Verma, S.B., 1992. Soil surface CO2 fluxes and the carbon budget of a grassland. J. Geophys. Res. 97 (D17), 18,845–18,853.
Notsu, K., Sugiyama, K., Hosoe, M., Uemura, A., Shimoike, Y., Tsunomori, F., Hernandez, P.A., 2005. Diffuse CO2 flux from Iwojima volcano of the Izu-Ogasawara arc, Japan. J. Volcanol. Geotherm. Res. 139, 147–161.
Oliveira, S., Viveiros, F., Silva, C., Pachenco, J.E., 2018. Automatic filtering of soil CO2 flux data: different statistical approaches applied to long time series. Front. Earth Sci. 6, 208. https://doi.org/10.3389/feart.2018.00208.
Pedone, M., Viveiros, F., Aiuppa, A., Giudice, G., Grassa, F., Gagliano, A.L., Francofonte, F., Ferreira, T., 2015. Total (fumarolic+ diffuse soil) CO2 output from Furnas volcano. Earth, Planets Space 67 (1), 1–12.
Pedone, M., Granieri, D., Moretti, R., Fedele, A., Troise, C., Somma, R., De Natale, G., 2017. Improved quantification of CO2 emission at Campi Flegrei by combined Lagrangian Stochastic and Eulerian dispersion modelling. Atmos. Environ. 170, 1–11.
Pereira, M.L., Matias, D., Viveiros, F., Moreno, L., Silva, C., Zanon, V., Uchôa, J., 2022. The contribution of hydrothermal mineral alteration analysis and gas geothermometry for understanding high-temperature geothermal fields - the case of Ribeira Grande geothermal field, Azores. Geothermics 105, 102519. https://doi.org/10.1016/j.geothermics.2022.102519.
Permentier, K., Vercammen, S., Soetaert, S., Schellemans, C., 2017. Carbon dioxide poisoning: a literature review of an often forgotten cause of intoxication in the emergency department. Int. J. Emerg. Med. 10, 14. https://doi.org/10.1186/s12245-017-0142-y.
Poret, M., Corradini, S., Merucci, L., Costa, A., Andronico, D., Montopoli, M., Vulpiani, G., Freret-Lorgeril, V., 2018. Reconstructing volcanic plume evolution integrating satellite and ground-based data: application to the 23 November 2013 Etna eruption. Atmos. Chem. Phys. 18 (7), 4695–4714.
Quartau, R., Hipólito, A., Mitchell, N.C., Gaspar, J.L., Brandão, F., 2015. Comment on Construction and destruction of a volcanic island developed inside an oceanic rift: Graciosa Island, Terceira Rift, Azores by Sibrant et al.(2014) and proposal of a new model for Graciosa's geological evolution. J. Volcanol. Geotherm. Res. 303, 146–156.

Rinaldi, A.P., Vandemeulebrouck, J., Todesco, M., Viveiros, F., 2012. Effects of atmospheric conditions on surface diffuse degassing. J. Geophys. Res. 117, B11201. https://doi.org/10.1029/2012JB009490.

Settimo, G., Turrio Baldassarri, L., Brini, S., Lepore, A., Moricci, F., de Martino, A., Casto, L., Musmeci, L., Nania, M.A., Costamagna, F., Marcello, I., Fuselli, S., 2016. Gruppo di Studio Nazionale sull'Inquinamento Indoor. In: Presenza di CO2 e H2S in ambienti indoor: conoscenze attuali e letteratura scientifica in materia. Istituto Superiore di Sanità (Rapporti ISTISAN 16/15), Roma.

Sinclair, A.J., 1974. Selection of threshold values in geochemical data using probability graphs. J. Geochem. Explor. 3, 129–149.

Viveiros, F., Ferreira, T., Cabral Vieira, J., Silva, C., Gaspar, J.L., 2008. Environmental influences on soil CO2 degassing at Furnas and Fogo volcanoes (São Miguel Island, Azores archipelago). J. Volcanol. Geotherm. Res. 177, 883–893. https://doi.org/10.1016/j.jvolgeores.2008.07.005.

Viveiros, F., Ferreira, T., Silva, C., Gaspar, J.L., 2009. Meteorological factors controlling soil gases and indoor CO_2 concentration: a permanent risk in degassing areas. Sci. Total Environ. 407, 1362–1372.

Viveiros, F., Cardellini, C., Ferreira, T., Caliro, S., Chiodini, G., Silva, C., 2010. Soil CO2 emissions at Furnas volcano, São Miguel Island, Azores archipelago: Volcano monitoring perspectives, geomorphologic studies, and land use planning application. J. Geophys. Res. 115, B12208.

Viveiros, F., Cardellini, C., Ferreira, T., Silva, C., 2012. Contribution of CO2 emitted to the atmosphere by diffuse degassing from volcanoes: the Furnas Volcano case study. Intern. J. Global Warm. 4 (3–4), 287–304.

Viveiros, F., Ferreira, T., Silva, C., Vieira, J.C., Gaspar, J.L., Virgili, G., Amaral, P., 2015a. Permanent monitoring of soil CO2 degassing at Furnas and Fogo volcanoes (São Miguel Island, Azores). Geol. Soc. Lond. Mem. 44, 271–288. https://doi.org/10.1144/M44.20.

Viveiros, F., Gaspar, J.L., Ferreira, T., Silva, C., Marcos, M., Hipólito, A., 2015b. Mapping of soil CO2 diffuse degassing at São Miguel Island and its public health implications. Geol. Soc. Lond. Mem. 44, 185–195. https://doi.org/10.1144/M44.14.

Viveiros, F., Gaspar, J.L., Ferreira, T., Silva, C., 2016. Hazardous indoor CO2 concentrations in volcanic environments. Environ. Pollut. 214, 776–786. https://doi.org/10.1016/j.envpol.2016.04.086.

Viveiros, F., Silva, C., Moreno, L., Pacheco, J.E., Ferreira, T., 2020a. Secondary manifestations of volcanism - an open window to understand geothermal resources in the Azores archipelago. Comun. Geol. 107 (Especial I), 89–91.

Viveiros, F., Chiodini, G., Cardellini, C., Caliro, C., Zanon, V., Silva, C., Rizzo, A.L., Hipólito, A., Moreno, L., 2020b. Deep CO2 emitted at Furnas do Enxofre geothermal area (Terceira Island, Azores archipelago). An approach for determining CO2 sources and total emissions using carbon isotopic data. J. Volcanol. Geotherm. Res. 401 https://doi.org/10.1016/j.jvolgeores.2020.106968.

Viveiros, F., Silva, C., Matias, D., Moreno, L., Driesner, T., Zanon, V., Uchôa, J., Cruz, J. V., Freire, P., Pereira, M.L., Pacheco, J., 2021. Geochemical tools as a contribution to improve geothermal potential on the Azores archipelago. In: Proceedings World Geothermal Congress 2020, Reykjavic, Iceland, 8.

Wallenstein, N., Duncan, A.M., Guest, J.E., Almeida, M.H., 2015. Eruptive history of Fogo Volcano, São Miguel, Azores. In: Gaspar, J.L., Guest, J.E., Duncan, A.M., Barriga, F.J.A.S., Chester, D.K. (Eds.), Volcanic Geology of S. Miguel Island (Azores archipelago). Geol. Soc., London Mem., London, pp. 105–123.

Werner, C., Brantley, S.L., Boomer, K., 2000. CO_2 emissions related to the Yellowstone volcanic system. Statistical sampling, total degassing, and transport mechanisms. J. Geophys. Res. 105, 10831–10846.

Werner, C., Fischer, T., Aiuppa, A., Edmonds, M., Cardellini, C., Carn, S., Chiodini, G., Cottrell, E., Burton, M., Shinoara, H., Allard, P., 2019. Carbon Dioxide Emissions from Subaerial Volcanic Regions: Two decades in Review. In: Orcutt, B., Daniel, I., Dasgupta, R. (Eds.), Deep Carbon: Past to Present. Cambridge University Press, Cambridge, pp. 188–236. https://doi.org/10.1017/9781108677950.008.

Williams-Jones, G., Rymer, H., 2000. Hazards of volcanic gases. In: Sigurdsson, H. (Ed.), Encyclopedia of Volcanoes. American Press, San Diego, pp. 997–1004.

Wong, K.L., 1996. Carbon Dioxide. Spacecraft Maximum Allowable Concentrations for Selected Contaminants, 2. National Academy of Sciences, USA, Washington DC, pp. 105–187.